Study on the Pharmacological Mechanism of the Xihuang Pill and its Treatment of Breast Cancer Based on Nontargeted Metabonomics

Yifan Su[1,2], Xiaohui Zhao[1,2], Dehui Li[1*], Jiao Liu[1,2] & Xu-kuo Liu[1,2]

[1]Hebei Province Hospital of Chinese Medicine; The First Affiliated Hospital of Hebei University of Chinese Medicine, Shi Jiazhuang, 050011, China.

[2]Graduate School of Hebei University of Chinese Medicine, Shijiazhuang 050091, China.

Yi-fan Su and Xiao-hui Zhao have contributed equally to this work and share first authorship. Yi-fan Su and Xiao-hui Zhao conducted most of the research, performed statistical analysis and wrote the manuscript.
De-hui Li designed the study and reviewed the manuscript.
Jiao Liu and Xu-kuo Liu helped in the animal study and recorded the data.

Abstract:

[Objective] To study the main differential metabolites of Xihuang Pill (XHP) in rat serum and the mechanism of related pathways of metabolites on breast cancer.
[Methods] Qualitative and quantitative analysis of metabolites in XHP drug serum group and blank serum group by liquid chromatography-mass spectrometry (LC-MS) technology. And using sample correlation heat map and multivariate statistical analysis methods to compare the metabolic differences between the two groups. The metabolites were analyzed by cluster analysis, Variable Importance in Projection (VIP) analysis, Kyoto Encyclopedia of genes and Genomes (KEGG) compound classification and KEGG functional and enrichment topology analysis.
[Results] LC-MS technology identified a total of 765 metabolites in the XHP drug serum group; a total of 697 metabolites in the blank serum group. VIP analysis screened the top 30 serum differential metabolites that were significantly different between the two groups, such as Abscisic acid, Quillaic acid, 2,2-Bis(4-hydroxyphenyl)-1-propanol, Corey PG-Lactone Diol, (S)-Naproxen and so on. KEGG compound classification showed that most of the metabolites in XHP were classified as phospholipids and amino acids, steroid hormones and carboxylic acids . KEGG functional pathways main involved are Lipid metabolism, Amino acid metabolism, Cancer: overview. KEGG enrichment and topology analysis, mainly involved in steroid hormone biosynthesis pathway and beta-alanine metabolism pathway.
[Conclusions] The main differential metabolite of XHP in rat serum may be Abscisic acid. XHP may exert its pharmacological effect on breast cancer by regulating steroid hormone biosynthesis pathway to regulate estrogen and progesterone levels and beta-alanine metabolism pathway to induce cancer cell apoptosis.

Keywords: Xihuang Pill; LC-MS; Metabolomics; Metabolite analysis

1. Introduction

Xihuang Pill (XHP) is from the "*waike zhengzhi quansheng ji*" compiled by Wang Weide in the Qing Dynasty. Its prescription consists of NIU HUANG, SHE XIANG, RU XIANG, and MO YAO[1]. As a classical prescription, XHP has been used in the clinical treatment of various diseases. XHP has good curative effects on breast cancer, liver cancer, gastric cancer, colon cancer, lung

*Corresponding author: Dehui Li (E-mail: 258289951@qq.com).
*This research was supported by the National Natural Science Foundation of China (Grants No. 81603412); Key r&d Projects of Hebei Province (Grants No. 18277731D); Scientific Research Project of Hebei Administration of Traditional Chinese Medicine (Grants No. 2017163, 2019008, 2020014, 2023045); General Projects for Improving Scientific Research Capacity of Hebei College of Traditional Chinese Medicine (Grants No. KTY2019009); Hebei Key Laboratory of Chinese Medicine Research on Cardio-Cerebrovascular Disease; Key Laboratory of Integrated Traditional Chinese and Western Medicine Hepatonephrosis in Hebei Province (Grants No. A201902). Hebei Province "three three three talent project" funded project (Grants No. A202002008). Scientific Research Project of Health Commission of Hebei Province (Grants No. 20220962).

cancer and other tumors[2]. Modern pharmacological research shows that XHP has antitumor, anti-inflammatory, antibacterial, and immune-enhancing effects[3]. Experiments have demonstrated that XHP can restrain the proliferation of tumor cells while promoting tumor cell apoptosis, preventing tumor invasion and metastasis, preventing tumor angiogenesis, and regulating the tumor microenvironment[4,5]. In the early stage, we mainly studied the mechanism of XHP in treating precancerous lesions of breast cancer. We used 7,12-dimethylbenzanthracene (DMBA) combined with estrogen and progesterone to induce a rat model of precancerous lesions of breast cancer and intervened with XHP. XHP may advance the apoptosis of precancerous cells and decrease the hyperplasia of vascular endothelial cells by regulating the expression of genes and proteins that have a bearing on the PI3K/AKT/mTOR pathway, thereby inhibiting the progression of precancerous lesions of breast cancer[6]. XHP may treat precancerous lesions of breast cancer by improving microcirculation in rats with precancerous lesions of breast cancer[7]. XHP can block and reverse the histopathology of breast tissue in rats with breast cancer precancerous lesions sequentially triggered by DMBA combined with estrogen and progesterone, and its mechanism may be related to its regulation of the expression of NF-κB protein in breast tissue[8]. In clinical studies, XHP combined with chemotherapy to treat breast cancer can enhance clinical efficacy, improve the quality of life, and reduce the untoward reactions caused by chemotherapy[9].

Metabolomics is used to detect the dynamic and overall changes in metabolites, obtain meaningful biomolecular information, and understand the biological process of the body under the actions of drugs[10]. Metabolomics helps to understand the relationship between traditional Chinese medicine (TCM) and diseases from the perspective of molecular biology and to study their mechanisms of action, which is conducive to the better efficacy of TCM in the body. Metabolomics is now widely used in the screening of active components of TCM and the study of the pharmacokinetics and mechanisms of action of TCM, providing a new method for the modernization of TCM[11]. Due to the multicomponent, multitarget and multimechanistic treatment of diseases by the Chinese medicine XHP, its complexity and the diversity of processes in the body make it difficult to deepen modern research on XHP, and the metabolites of XHP are not yet clear. To solve this problem, this article mainly applies LC–MS technology to carry out nontargeted metabolomic analysis of the components of XHP. To explore the main differential metabolites of XHP, metabolites were classified, and their relationships with diseases were evaluated. Studying the differential metabolites of XHP is of great significance for a comprehensive understanding of their pharmacological mechanisms in the treatment of breast cancer.

2. Materials

2.1 Instruments and Equipment

NewClassic MS electronic balance (NewClassic MF MS105DU, METTLER TOLEDO); Freezing centrifuge (Centrifuge 5424 R, Eppendorf); Temperature Control Ultrasonic Cleaner-10L (SBL-10TD, Ningbo Xinzhi Biological Technology Co., Ltd.); Multi sample freeze grinder (Wonbio-96c, Shanghai Wanbai Biotechnology Co., Ltd); Bench type rapid centrifugal concentration dryer (LNG-T88, Taicang Huamei biochemical instrument factory); Nitrogen purging instrument (JXDC-20, Shanghai Jingxin Industrial Development Co., Ltd); UHPLC liquid chromatography system (Vanquish Horizon system, Thermo Scientific); Mass spectrometer (Q-Exactive, Thermo Scientific).

2.2 Drugs and Reagents

XHP (Zhejiang Tianyitang Pharmaceutical Co., Ltd. Division, lot No.: 1703011); Methanol

(Fisher Chemical); Acetonitrile (Fisher Chemical); Formic Acid (CNW); Water (Fisher Chemical); 2-Propanol (Merck); 2-Chloro-L-Phenylalanine (Adamas-beta).

2.3 Animals and Groups

Twelve SPF 6-week-old female Sprague–Dawley (SD) rats (weighing 180 ± 20 g) were purchased from Hebei Experimental Animal Center (Shijiazhuang, Hebei, China, license number: 1705351). Animal experiments were approved by the Medical Ethics Committee of Hebei University of Chinese Medicine and were carried out in accordance with the Animal Welfare Guidelines of the Medical Ethics Committee of Hebei University of Chinese Medicine (ethical review number: DWLL2019036). The rats were divided into two groups: an XHP drug serum group and a blank serum group, with six rats in each group. The rats in the two groups were allowed to feed and drink freely, and the experiment was carried out after 1 week of routine feeding.

3. Methods

3.1 Preparation of Serum

3.1.1 Preparation of XHP Drug Serum

The rats in the XHP-containing serum group were given XHP Chinese medicine solution every day. XHP was ground, crushed and made into a suspension with distilled water. The concentration was 0.25 g/ml, and the administration volume was 5 ml/kg. It was administered twice a day. The cumulative daily dose was 2.5 g/kg. Dose conversion between humans and rats was carried out with reference to the “Methodology of Pharmacological Research of Traditional Chinese Medicine” edited by Chen Qi. It was administered by gavage according to the dose for 3 days. One hour after the last administration on the 4th day (after fasting for 12 h prior to gavage), the rats were anesthetized with pentobarbital sodium 200 $mg \cdot kg^{-1}$, ip, blood was collected from the abdominal aorta, and serum was separated in a sterile tube. After the serum was inactivated at 56 ºC for 30 min, it was stored at -80 °C for later use.

3.1.2 Preparation of Blank Serum

The rats in the blank serum group were administered distilled water ig every day (the dosage volume was the same as that in the XHP drug serum group). For 3 consecutive days, blood was collected and separated at the same time as that in the XHP drug serum group. The method of serum preservation was the same as that in the XHP drug serum group.

3.2 Serum Grouping

Two hundred microliters of serum from each rat in the XHP serum and blank serum groups was extracted for LC–MS metabolomics analysis. The drug serum extracted from the XHP-containing serum group was set as the experimental group (sy), and the sy group was divided into experimental Group 1 (sy1), experimental Group 2 (sy2), experimental Group 3 (sy3), experimental Group 4 (sy4), experimental Group 5 (sy5) and experimental Group 6 (sy6). The serum of the blank serum group was set as the control check (ck), and ck group was divided into control check 1 (ck1), control check 2 (ck2), control check 3 (ck3), control check 4 (ck4), control check 5 (ck5) and control check 6 (ck6). The above experimental group included 6 groups, and the control group included 6 groups. LC–MS nontargeted metabolomics analysis and multivariate statistical analysis were performed to compare the metabolic differences between the two groups.

3.3 LC–MS Analysis

3.3.1 Sample Treatment

We accurately removed 100 μL serum from each group to a 1.5 mL centrifuge tube and added 400 μL extract (methanol:acetonitrile = 1:1 (v:v)) containing 0.02 mg/mL internal standard

(L-2-chlorophenylalanine); after vortex mixing for 30 s, we performed low-temperature ultrasonic extraction for 30 min (5 °C, 40 kHz), placed the sample at -20 °C for 30 min, centrifuged for 15 min (13000 × g, 4 °C), took supernatant and dried the sample with nitrogen, added 120 μL reconstituted solution (acetonitrile:water = 1:1) to reconstitute, vortexed and mixed for 30 s, followed by low-temperature ultrasonic extraction for 5 min (5 °C, 40 kHz), centrifuged for 10 min (13000 × g, 4 °C), and transferred the supernatant to an injection vial with an inner cannula for analysis. In addition, 20 μL of the supernatant was pipetted for each sample and mixed as a quality control sample.

3.3.2 Chromatographic Conditions

The chromatographic column was an ACQUITY UPLC HSS T3 (100 mm × 2.1 mm i.d., 1.8 μm; Waters, Milford, USA); mobile phase A was 95% water + 5% acetonitrile (containing 0.1% formic acid), and mobile phase B was 47.5% acetonitrile + 47.5% isopropanol + 5% water (containing 0.1% formic acid). The flow rate was 0.40 mL/min, the injection volume was 2 μL, and the column temperature was 40 °C.

3.3.3 Mass Spectrometry Conditions

The sample was electrospray ionized, and mass spectrometry signals were collected in positive and negative ion scanning modes. The scan type parameter was 70-1050 m/z; the sheath gas flow rate parameter was 40 arb; aux gas flow rate parameter was 10 arb; the heater temp parameter was 400 ºC; the capillary temp parameter was 320 ºC; the spray voltage (+) parameter was 3500 V; the spray voltage (-) parameter was -2800 V; the s-Lens RF Level parameter was 50; the normalized collision energy was 20, 40, and 60 eV; the resolution (Full MS) was 70000; and the resolution (MS2) was 17500.

3.3.4 Preparation of Quality Control Samples

Quality control (QC) samples were prepared by mixing the extracts of all samples in equal volumes. The volume of each QC was the same as that of the sample. It was processed and tested in the same way as the analysis sample. QC was injected every 4 samples to check the stability of the whole detection process. Therefore, the quality control samples of this experiment are divided into quality control sample 1, quality control sample 2, and quality control sample 3.

3.4 Data Analysis

Thermo Fisher's Ultra High-Performance Liquid Chromatography tandem Fourier Transform mass spectrometry UHPLC-Q Exactive system was used for chromatographic peak identification. Progenesis QI software (Waters Corporation, Milford, USA) was used to perform baseline filtering, peak identification, integration, retention time correction, and peak alignment to obtain information such as the mass-nucleus ratio (m/z), retention time and peak area. Then, the software was used to search and identify the characteristic peaks, and the MS and MS/MS mass spectral information was matched with the metabolic database. The MS mass error was set to be less than 10 ppm, and the metabolites were identified according to the secondary MS spectrometry matching score. The main databases were http://www.hmdb.ca/, https://metlin.scripps.edu/and additional mainstream public databases and self-built databases. The normalized data matrix was imported into the Ropls software package for pattern recognition analysis of PCA and OPLS-DA. Analysis software platforms and related versions involved in this paper see Table 1.

4. Results

4.1 Venn Analysis of Differential Metabolites

The substances detected by the mass spectrometer were obtained through LC–MS analysis

(Supplementary Table S1). Through primary and secondary mass spectrometry data, libraries (self-built database, Metlin database, HMDB database, etc.) were searched to finally obtain the annotated substances. See Supplementary Tables S2 and S3 for the metabolite information of the experimental and control groups, respectively. A total of 765 XHP metabolites were identified in the serum of the experimental group; 697 serum metabolites were identified in the control group. The obtained metabolite data of the experimental and control groups were imported into Venn Diagram (R package) software, and the intersection was taken to obtain the coacting metabolites. Venn diagram analysis revealed the number of metabolites and the overlapping relationships of metabolites in each group. The results showed that among the positive ion metabolites, there were 396 in the control group and 442 in the experimental group, and the intersection of the two positive ion metabolites yielded 396; among the negative ion metabolites, there were 301 in the control group and 323 in the experimental group, and the intersection of the two negative ion metabolites yielded 301. The results are summarized in Figure 1.

4.2 Comparison and Screening of Two Groups of Differential Metabolites by

4.2.1 Difference Statistics and Volcano Map

The two groups of differential metabolites were compared and graphed, as shown in Figure 2. The X-axis is the multiple shift value of the metabolite expression difference between the two groups, i.e., log2FC, and the Y-axis is the statistical test value of metabolite expression difference, i.e., -log10 (*p*_value). The higher the value is, the more remarkable the expression discrepancy is. The values of the X- and Y-axes are logarithmic. Every point in the figure represents a given metabolite, and the point size represents the VIP value size. The point on the left is the metabolite of differentially downregulated expression, and the point on the right is the metabolite of differentially upregulated expression. The closer it is to the left, right and upper points, the more remarkable the expression discrepancy. The results showed that the experimental and control groups were significantly different. There were 115 positive ions and 87 negative ions of differential metabolites, and the expression levels of differential metabolites were upregulated more than downregulated. See A, B and C in Figure 2.

4.2.2 Details of the Differences Between Groups

The differential metabolism between the groups was studied, and a histogram of the relative expression abundance of metabolites in each group of samples was obtained. The difference test methods included the Student's t test (Unpaired) using a two-tailed test; OPLS-DA data conversion was performed using Pareto transformation, for which the OPLS-DA confidence level was 0.95, and the OPLS-DA number of permutations was 200 (P value < 0.05, VIP pred OPLS-DA > 1, display FC value: > 1 or < 1). The Y coordinate is the mass spectrum intensity value (the mass spectrum intensity after data preprocessing), and the error bars represent the average value±standard deviation. The VIP value was selected according to OPLS-DA in descending order, and the largest metabolite was selected for differential metabolism analysis, as shown in D, E and F in Figure 2. Abscisic acid is the metabolite with the largest difference between the experimental and control groups in positive ion mode and positive-negative ion mode. In negative ion mode, (S)-naproxen was the metabolite with the greatest difference between the experimental and control groups. The contents of these two metabolites in the experimental group were greater than those in the control group.

4.2.3 PCA Analysis

The PCA method was used to analyze the LC/MS data of the experimental and control groups.

Then, the samples were analyzed by dimensionality reduction. The PCA results in positive and negative ion modes are shown in Figure 3, A and B, respectively. The experimental and control groups showed obvious separation trends, indicating that the metabolites of the two groups were significantly different. The two sets of samples could be separated by PCA. The confidence ellipse implies that the "true" samples of this group are distributed in this area with a 95% confidence level; more than this area can be considered a probable abnormal sample. Panels A and B in Figure 3 show that no abnormal samples that deviated from the confidence circle were detected in the LC–MS. Green dots, control group; blue triangles, experimental group.

4.2.4 PLS-DA Analysis

The LC/MS data of the two groups of samples were analyzed by the PLS-DA method, and the samples were analyzed by dimensionality reduction. The PLS-DA analysis results in positive and negative modes are shown in Figure 4, A and B, respectively. The experimental and control groups showed obvious separation trends, indicating that the metabolites of the two groups were significantly different.

The serum metabolic profiles of the two groups showed significant separation in positive and negative ion modes. To test the reliability of the model and prevent overfitting, the model overview and displacement test chart were used for verification. The PLS-DA model is shown in panels C and D in Figure 4. There were two principal components in the positive ion model: the model interpretation rate R^2X was 0.407, the predictive ability parameter Q^2 was 0.953, and $Q^2 > 0.5$, indicating that the model had a better predictive ability and a better fit. There were two principal components in the negative ion model: the model interpretation rate R^2X was 0.523, the predictive ability parameter Q^2 was 0.966, and $Q^2 > 0.5$, indicating an excellent degree of fit.

In the displacement test, the abscissa represents the displacement retention, the ordinate represents the values of the R^2 (red dots) and Q^2 (blue triangles) displacement tests, and the two dotted lines represent the regression lines of R^2 and Q^2, respectively. Permutation tests were performed for the experimental and control groups. The replacement test model randomly disrupts the grouping labels (Y variables) of the experimental and control groups. The replacement retention of the horizontal axis was the proportion consistent with the order of the Y variables of the original model. The replacement retention was 1, that is, R^2 and Q^2 of the original PLS-DA model. The number of random permutation tests was 200, R^2 was 0.8818, and Q^2 was -0.0401 (negative ion model). R^2 was 0.9435, and Q^2 was -0.0710 (positive ion model). The negative value of Q^2 indicated that the model built was reliable, there was no overfitting phenomenon, and the modeling was successful. As the replacement retention decreased, the regression line showed an upward trend, indicating that the replacement test was passed (Figure 4, E and F).

4.2.5 OPLS-DA Analysis

The OPLS-DA score map filters out information irrelevant to the grouping through orthogonal rotation, thereby better making a distinction between groups and improving the function of the model. The OPLS-DA results in positive and negative modes are shown in Figure 5, A and B, respectively. The experimental and control groups showed obvious separation trends, indicating that the metabolites of the two groups were significantly different.

To verify the reliability of the model and prevent overfitting, the model overview and permutation test chart were used for verification. The OPLS-DA model, is shown in panels C and D in Figure 5. There were two principal components in the positive ion model: the model interpretation rate R^2X was 0.407, the predictive ability parameter Q^2 was 0.919, and $Q^2 > 0.5$, indicating that the model

had a better predictive ability and a better fit. There were two principal components in the negative ion model: the model interpretation rate R^2X was 0.523, the predictive ability parameter Q^2 was 0.96, and $Q^2 > 0.5$, indicating an excellent degree of fit.

In the displacement test, the abscissa represents the displacement retention, the ordinate represents the values of the R^2 (red dots) and Q^2 (blue triangles) displacement tests, and the two dotted lines represent the regression lines of R^2 and Q^2, respectively. The number of random permutation tests was 200, R^2 was 0.8811, and Q^2 was -0.0948 (negative ion model). R^2 was 0.943, and Q^2 was -0.0607 (positive ion model). The negative value of Q^2 indicated that the model built was reliable, there was no overfitting phenomenon, and the modeling was successful. As the replacement retention decreased, the regression line showed an upward trend, indicating that the replacement test was passed (Figure 5, E and F).

4.3 Cluster Analysis of Metabolites

Hierarchical cluster analysis was carried out on the different metabolites in the experimental and control groups. The metabolite clustering analysis algorithm was based on hierarchical clustering. The subclusters were used select the top ten, and the top 30 most abundant metabolites were selected, as shown in Figure 6. On the left is a dendrogram of metabolite clustering, and the metabolite name is on the right. The closer the two metabolite branches are, the more similar their expression levels are; the dendrogram of sample clustering is at the top, and the name of the sample is at the bottom. The closer the two sample branches are, the closer the expression pattern of all metabolites of the two samples is, that is, the closer the shift trend of metabolite expression is. The metabolite expression trends of the control group and the experimental group were different. In the control group, the expression levels of 2-indolecarboxylic acid and indole-3-carboxilic acid-O-sulfate in subcluster 5 and carboxyoprost bromethamine in subcluster 8 and (±)-propionylcarnitine in subcluster 10 were upregulated, while other subclusters were downregulated. The expression levels of the remaining metabolites were upregulated in the experimental group.

4.4 Variable Importance in Projection (VIP) Value Analysis

According to the weighting coefficient of the OPLS-DA model, the VIP score was used to rank the identification contributions of the metabolites in the experimental and control groups. The metabolite clustering algorithm was hierarchical clustering, the metabolite distance algorithm was Euclidean, the metabolite hierarchical clustering method was complete, the VIP value was derived from OPLS-DA, VIP ≥ 1, and the metabolites with the top 30 VIP values were selected. As shown in Figure 7, a higher VIP value indicated that the metabolite differed greatly between the two groups. The top five metabolites were abscisic acid (VIP = 6.1604), quillaic acid (VIP = 6.0746), 2,2-bis(4-hydroxyphenyl)-1-propanol (VIP = 5.543), Corey PG-lactone diol (VIP = 5.4712) and (S)-naproxen (VIP = 4.7948). The selected differential metabolites are shown in Table 2.

4.5 KEGG compound classification

Kyoto Encyclopedia of Genes and Genomes (KEGG) compound classification is based on compounds with biological roles. The identified metabolites were compared to the KEGG Compound database to obtain the metabolite classification profile and statistical mapping. KEGG compound classification revealed that the metabolite classification in XHP consisted of mostly phospholipids (22 metabolites), amino acids (14 metabolites), steroid hormones (6 metabolites) and carboxylic acids (5 metabolites), as shown in Figure 8.

4.6 KEGG functional pathway analysis

By comparing the results with the KEGG database, the metabolites in the experimental group can be sorted in light of the pathways touched upon or the functions they perform. As shown in Figure 9, the main pathways involved included lipid metabolism (64 metabolites), amino acid metabolism (44 metabolites), cancer: overview (41 metabolites), digestive system (28 metabolites), metabolism of other amino acids (16 metabolites), nervous system (15 metabolites), and membrane transport (15 metabolites). XHP had the characteristics of multicomponent, multitarget and multilink overall effects. To further study the mechanism of XHP in treating breast cancer, we sorted out the metabolites (15 numbers) that XHP significantly regulated that were related to breast cancer and their functional predictions (see Supplementary Table S4).

4.7 KEGG Pathway Enrichment Analysis

Through KEGG enrichment and topological analyses, 13 different metabolic pathways were found, as shown in Figures 10 and 11. KEGG enrichment analysis showed that the two groups had significant changes in the following pathways: necroptosis, steroid hormone biosynthesis, beta-alanine metabolism, vitamin digestion and absorption, and apoptosis. Topological analysis revealed 4 main metabolic pathways, namely, steroid hormone biosynthesis, beta-alanine metabolism, retinol metabolism, and caffeine metabolism. The metabolic pathways with statistically significant differences ($P < 0.05$) were the steroid hormone biosynthesis pathway and the beta-alanine metabolism pathway. The steroid hormone biosynthesis pathway included three metabolites: 21-hydroxypregnenolone (c05485), corticosterone (c05488) and 21-deoxycytortisol (c05497). The beta-alanine metabolism pathway included two metabolites: carnosine (c00386) and pantothenic acid (c00864). See Figure 12.

5. Discussion

With the gradual deepening of biotechnology research, some molecular compounds have been found to have impacts on some diseases. For example, F. S. Mohammed et al.[12] showed that sechium edule extract results in the prolongation of QT or QTc and RR intervals and increases the heart rate in high-fat diet-challenged mice. S. Taifa et al.[13] found that copper nanoparticles have an excellent effect on mastitis. This article studies the metabolic compounds of XHP and the mechanisms of its metabolites in the treatment of breast cancer. XHP is composed of NIU HUANG, SHE XIANG, RU XIANG, and MO YAO. It is a commonly used Chinese patent medicine for the treatment of tumors, especially breast cancer and other diseases. In recent years, there have been many pharmacological studies on the four traditional Chinese medicines in XHP. These studies have shown that NIU HUANG and SHE XIANG inhibit the proliferation of cancer cells[14, 15]. In addition, the active ingredients in NIU HUANG can reduce the proliferation of human colon adenocarcinoma cells[16]. Deoxycholic acid, a component of NIU HUANG, can block cells in G2/M phase, inhibit the growth of human gastric cancer BGC-823 cells and induce apoptosis through the mitochondrial pathway[17]. Muskone, the active ingredient in SHE XIANG, can significantly inhibit the expression of basic fibroblast growth factor and vascular endothelial cell growth factor in the nude mouse model of breast cancer MDA231 cell line, thereby inhibiting tumor angiogenesis[18]. RU XIANG and MO YAO can promote the apoptosis of cancer cells[19]. The main antitumor components of RU XIANG are boswellic acids, which have various effects, such as reducing the proliferation of cancer cells, promoting their apoptosis, and intervening to attenuate the conduction of tumor-related signaling pathways[20].

At present, the pharmacological mechanism of XHP based on nontargeted metabolomics has not been found. Therefore, this study used nontargeted metabolomics to analyze the metabolites of

XHP in rat serum. Mass spectrometry (MS) and nuclear magnetic resonance (NMR) are the two most widely used techniques for compound identification. In compound analysis, MS and NMR are complementary relationships. MS can provide the atomic formula of an analyte, while NMR provides the structural parts into which these atoms are organized. For example, NMR can distinguish between isobaric compounds and positional isomers. MS can recognize certain functional groups, such as sulfate and nitro groups. These complementary capabilities of MS and NMR mean that neither detector can be employed alone for comprehensive compound analysis in the fields of natural product discovery, metabolomics, and drug metabolite identification[21]. As an analytical platform, NMR is a powerful tool for studying the structure and dynamics of biomolecules under physiological conditions[22]. NMR can play an essential role in drug discovery because of its ability to provide protein–ligand binding information in solution[23]. NMR is the earliest technique to measure metabolites in biological specimens, and this technique has been successfully applied in selecting tumor markers, judging prognosis, pathological typing, and early diagnosis[24]. The advantages of NMR techniques include selective isotopic detection in complex mixtures, determination of unknown key structural parameter metabolites, inherent quantification, in situ analysis of pathway dynamics from cells to whole organisms, and nondestructive effects[25]. However, NMR has many shortcomings: the spectral resolution is not high, and it does not have the function of chromatographic separation; moreover, the derived spectrum is affected by the mutual interference of the peaks of various compounds, so the analytical results are limited, and its sensitivity is also lower than that of LC–MS[26]. LC–MS can make up for these two deficiencies at the same time and can be used to conduct more accurate qualitative and quantitative analyses of target compounds in samples.

Through nontargeted metabolomic analysis, we identified a total of 765 metabolites in the XHP drug serogroup and 697 metabolites in the blank serogroup. The two groups were compared by multivariate statistical analysis, and the results showed that there were metabolite differences between the two groups. In this study, through the comparison of different metabolites between the two groups, it was found that abscisic acid and (S)-naproxen were significantly different between the two groups, and the contents of the two metabolites in the XHP drug serum group were higher than those in the blank serum group and may be the main functional components of XHP in blood metabolism and circulation. VIP analysis found that abscisic acid, quillaic acid, 2,2-bis(4-hydroxyphenyl)-1-propanol, Corey PG-lactone diol and (S)-naproxen were significantly different in the two groups. Therefore, abscisic acid and (S)-naproxen may be the main differential metabolites between the two groups. Abscisic acid is a plant hormone that exists not only in plants but also in humans and animals. In mice, abscisic acid reduces obesity and interferes with insulin resistance. Abscisic acid can inhibit the proliferation of various cancer cells and induce apoptosis, induce the growth of mesenchymal stem cells and promote the growth of hematopoietic progenitor cells, and play a certain anti-inflammatory role in the immune system. Therefore, abscisic acid may be a potential drug for the treatment of various diseases[27]. Domestic and foreign studies have found that abscisic acid can resist tumors and inhibit the formation of blood vessels around tumors. Recent studies have found that abscisic acid can also be produced by mammalian cells and can inhibit the proliferation of cancer cells and regulate the dormancy of cancer cells in the bone marrow[28-30]. H. W. Zhao et al.[28] found that abscisic acid can enhance the activity of Caspase-3 in cancer cell lines, increase cancer cell apoptosis, slow down the growth of human tongue cancer Tca8113 xenografts, and induce differentiation. D. S. Jang et al.[31] found that abscisic acid

induced an increase in the content of quinone reductase, which could inhibit the growth of Hepa 1c1c7 hepatoma.

(S)-Naproxen is a nonsteroidal anti-inflammatory drug that can reduce the synthesis of thromboxane, prostacyclin and prostaglandin from arachidonic acid by inhibiting the cyclooxygenase subtype and has anti-inflammatory, analgesic and antipyretic pharmacological effects[32]. It is used in the treatment of chronic arthritis, osteoarthritis, ankylosing spondylitis, gout, and other conditions[33]. (S)-Naproxen exerts its anticancer adjuvant effect only by inhibiting the activation of cyclooxygenase-2. Its inhibition of cyclooxygenase-1 can induce the synthesis of prostaglandin E in the gastric mucosa, resulting in adverse reactions such as gastrointestinal tract upset[34]. Z. J. Li et al.[35] found that cisplatin compounds containing naproxen structures showed special antitumor activity, and the in vitro cytotoxicity of cisplatin coupled with naproxen structures on the breast tumor cell lines MCF-7 and MDA-MB-231 was stronger than that of cisplatin alone. In conclusion, abscisic acid and (S)-naproxen have inhibitory effects on the progression of breast cancer to a certain extent, but the specific mechanism needs to be further explored.

The functional KEGG pathways mainly involve lipid metabolism and amino acid metabolism. Modern studies have found that lipid metabolism and amino acid metabolism pathways have certain inhibitory effects on breast cancer. The regulation of lipid metabolism, such as lipid uptake, synthesis, and hydrolysis, is critical for maintaining cellular homeostasis[36]. Dysregulation of lipid metabolism is one of the most prominent metabolic alterations in cancer. Cancer cells utilize lipid metabolism for energy, biofilm composition, and signaling molecules required for proliferation, survival, invasion, metastasis, and response to tumor microenvironment influences and cancer therapy[37]. Cancer cells in the tumor microenvironment constantly change nutrient availability during tumor progression, utilizing lipid metabolism to support their rapid proliferation, survival, migration, invasion, and metastasis. Lipid metabolism is one of the conditions for tumor invasion and metastasis by increasing the decomposition of lipids. The lipids of tumor cells are composed of adipocytes, and fatty acid derivatives produced by the decomposition of adipocytes can enhance the invasiveness of breast cancer[38]. By studying the relationship between menopause and tumor development, Y. Dunneram found that women have a decrease in estrogen after menopause, which may lead to changes in fat metabolism and promote breast cancer[39]. If a woman's estrogen levels drop significantly after menopause, this hormonal change is likely to lead to a disorder of lipid metabolism. Therefore, postmenopausal women are more prone to visceral lipid accumulation than premenopausal women, and the increase in fatty acid derivatives produced by its decomposition can induce an increased risk of cancer[40]. Estrogen receptor-positive breast cancer is more dependent on estrogen and lipid metabolism. Therefore, the lipid metabolism pathway may be closely related to the development of and changes associated with breast cancer, regulating lipid metabolism, inhibiting the decomposition of fat cells, and helping to inhibit the growth and metastasis of breast cancer.

Modern research has found that amino acid metabolism is involved in tumor growth, amino acids are essential for the survival of tumor cells, and tumor cells have an increased demand for nutrients to promote proliferation and cancer progression. The more amino acids the body ingests, the stronger the tumor's proliferation ability. Recent studies have shown that the amino acid metabolism pathway is altered in breast cancer and that amino acid transporters influence tumor growth and progression. In breast cancer, glutamine is one of the key nutrients, and glutamine

metabolism is closely related to amino acid transporters[41]. The proliferation of cancer cells depends on the synthesis of intracellular nucleotides and the continuous replication of DNA. Glutamine, serine, glycine and aspartic acid are amino acid raw materials necessary for nucleotide synthesis, and serine is involved in DNA methylation. Arginine, leucine and glutamine act as signaling factors to activate the mammalian target of rapamycin signaling pathway. This pathway is closely related to tumor growth regulation, so the mechanism by which this pathway regulates tumors can be studied from the aspect of amino acids. The proliferation and maintenance of tumor cells are dependent on the supply of amino acids to the intracellular space, which is regulated by amino acid transporters. The development and changes of tumors are caused by many pathological molecular mechanisms induced by various factors, and the related mechanisms involved in amino acid metabolism include oncogene activation, related protein expression, cancer cell proliferation, cancer cell proliferation and metastasis, immune suppression, and immune escape[42].

KEGG enrichment and topological analysis showed that XHP was mainly involved in the steroid hormone biosynthesis and beta-alanine metabolism pathways. The three XHP metabolites involved in the steroid hormone biosynthesis pathway in this study were 21-hydroxypregnenolone, 21-deoxycortisol, and corticosterone. 21-Hydroxypregnenolone is involved in the synthesis of steroid hormones and can prevent fatigue and reduce stress[43]. 21-Deoxycortisol is a precursor of steroid hormones, and corticosterone is a steroid hormone and a key substance in the biosynthetic pathway of steroid hormones. Steroid hormones are fat-soluble hormones, and according to their pharmacological effects, they are divided into two cholesterol derivatives: adrenal cortex hormones and sex hormones. Steroid hormones can enter target cells by diffusion or carrier transport, and after entering cells, they bind to receptors to form hormone-receptor complexes and play roles in regulating gene expression. The synthesis of steroid hormones usually takes place in the adrenal cortex, gonads, brain, placenta, and adipose tissue, and two types of enzymes are mainly involved in their synthesis: cytochrome P450 enzymes and hydroxysteroid dehydrogenases[44]. Steroid hormones play important roles in regulating hormone-dependent tumor development, maintaining fluid balance, regulating immunity, and mediating changes in body metabolism and the stress response [44]. The secretion and growth of SHE XIANG are related to the biosynthesis of steroid hormones[45]. RU XIANG and MO YAO participated in the biosynthesis of steroid hormones in the treatment of breast hyperplasia[46]. Steroid hormones play prominent roles in the pathogenesis and progression of breast cancer. The steroid hormones estrogen and progesterone may induce breast cancer progression by increasing breast cancer stem cells[47]. In clinical applications, hormone replacement therapy (HRT) is used to treat sex hormone-dependent tumors[48]. The steroid hormone biosynthesis pathway synthesizes estrogen and progesterone, and modern studies have shown that estrogen can promote the proliferation of estrogen receptor-positive breast cancer cells. Therefore, by inhibiting this pathway, reducing estrogen production may inhibit the proliferation of estrogen–progesterone receptor-positive breast cancer cells. Whether XHP affects the occurrence and development of estrogen–progesterone receptor-positive breast cancer by regulating the steroid hormone biosynthesis pathway is worthy of further experimental investigation.

The two XHP metabolites involved in the beta-alanine metabolism pathway in this study were carnosine and pantothenic acid. Modern research has found that beta-alanine is a unique β-type amino acid in the body and does not participate in protein synthesis. Cytosine and uracil are metabolized to obtain beta-alanine[49], and the precursor substance beta-alanine is involved in the

synthesis of coenzyme a and pantothenic acid and combines with histidine to form carnosine and its derivative anserine[50, 51]. Therefore, in the beta-alanine metabolism pathway, carnosine, pantothenic acid and beta-alanine are closely related. Carnosine helps to inhibit tumor proliferation, and with the accumulation of carnosine, tumor growth is significantly inhibited. The reason is believed to be that the accumulation of carnosine hinders glycolysis and energy production[52]. Beta-alanine can transmit information between neurons and can also regulate hormones. It is an intermediate metabolite of various active substances[53] and regulates various physiological functions, such as metabolism in the body[50]. Beta-alanine metabolism may be involved in the apoptosis pathway. B. Saunders et al.[54] found that in the early stage of apoptosis, the continuous increase in beta-alanine content can cause oxidative stress damage to the brain, but it can increase the level of carnosine in muscles and relieve soreness. T. Gemelli et al.[55] showed that the gradual increase in the content of beta-alanine in the body will reduce the activities of the two main enzymes in glycolytic enzymes, pyruvate kinase and lactose dehydrogenase, thereby destroying the glycolysis process and inducing apoptosis. Y. Xu showed[56] that XHP can regulate beta-alanine, inhibit the expression of lactate dehydrogenase in breast cancer 4T1 cells, reduce the increase in cancer cells, and promote cell apoptosis. Therefore, XHP may induce breast cancer cell apoptosis by regulating the beta-alanine metabolism pathway.

6. Conclusion

In conclusion, this study used LC–MS technology to study the difference between the metabolites in the XHP and blank serum groups. After comparative analysis, a total of 30 different metabolites were obtained. Abscisic acid and (S)-naproxen were the main differential metabolites. Most of the metabolites were classified into phospholipids and amino acids, steroid hormones and carboxylic acids. The major pathways involved in the KEGG functional pathway were lipid metabolism, amino acid metabolism, and cancer. Thirteen KEGG enrichment pathways were identified, and the steroid hormone biosynthesis pathway and the beta-alanine metabolism pathway were the main pathways involved in tumor proliferation, differentiation and apoptosis. The metabolic changes of XHP in rats can elucidate the nature of the main differential metabolites and the main metabolic pathways involved, allowing a more in-depth study of XHP in the treatment of breast cancer and other tumors.

Data Availability

Data can be obtained from the author upon reasonable request.

Conflict of Interest

All authors declare no conflicts of interest.

Author Contributions

Yi-fan Su and Xiao-hui Zhao have contributed equally to this work and share first authorship. Yi-fan Su and Xiao-hui Zhao conducted most of the research, performed statistical analysis and wrote the manuscript. De-hui Li designed the study and reviewed the manuscript. Jiao Liu and Xu-kuo Liu helped in the animal study and recorded the data. All authors have read and agreed to the published version of the manuscript.

Funding

This research was supported by the National Natural Science Foundation of China (Grants No. 81603412); Key r&d Projects of Hebei Province (Grants No. 18277731D); Scientific Research Project of Hebei Administration of Traditional Chinese Medicine (Grants No. 2017163, 2019008, 2020014, 2023045); General Projects for Improving Scientific Research Capacity of Hebei College of Traditional Chinese Medicine (Grants No. KTY2019009); Hebei Key Laboratory of Chinese Medicine Research on Cardio-Cerebrovascular Disease; Key Laboratory of Integrated Traditional Chinese and Western Medicine Hepatonephrosis in Hebei Province (Grants No. A201902). Hebei Province "three three three talent project" funded project (Grants No. A202002008). Scientific Research Project of Health Commission of Hebei Province (Grants No. 20220962).

Acknowledgment

We would like to thank Majorbio Cloud Platform (www. majorbio.com) for its help in data analysis.

Supplementary Materials

Supplementary Tables 1: Substances detected by the mass spectrometer. Supplementary Tables 2: Summary of metabolite information for experimental groups. Supplementary Tables 3: Summary of metabolite information for the control group. Supplementary Table 4: The metabolites (15 numbers) that XHP significantly regulated and related to breast cancer and their function predictions. (*Supplementary Materials*)

References

[1] Li DH, Fan HF, Dong JF, et al. Based on BATMAN-TCM to Explore the Molecular Mechanism of Xihuang Pill Regulating Immune Function to Treat Breast Precancerous Lesions. Breast cancer (Dove Medical Press) 2021;13:725-742.

[2] Yang YT, Zeng J, Chen P, et al. Anti-tumor Application and Pharmacological Mechanism of Xihuangwan: A Review. Chinese Journal of Experimental Traditional Medical Formulae 2022;28(3):250-258.

[3] Xia SL, Wang X, Zhai YC, Liu JN, and Han T. Anti-tumor Mechanism of Xihuangwan and Research Progress on Its Combined Use in Anti-tumor Treatment. Chinese Journal of Experimental Traditional Medical Formulae 2021;27(6):217-225.

[4] Su L, Jiang YM, Xu Y, et al. Xihuang pill promotes apoptosis of Treg cells in the tumor microenvironment in 4T1 mouse breast cancer by upregulating MEKK1/SEK1/JNK1/AP-1 pathway. Biomedicine & pharmacotherapy 2018;102:1111-1119.

[5] Li XY, Su L, Jiang YM, et al. The Antitumor Effect of Xihuang Pill on Treg Cells Decreased in Tumor Microenvironment of 4T1 Breast Tumor-Bearing Mice by PI3K/AKT~AP-1 Signaling Pathway. Evidence-based complementary and alternative medicine 2018;2018:Article ID 6714829, 13 pages.

[6] Fan HF, Li DH, Guo N, et al. Xihuang Pill inhibits the development of DMBA combined estrogen and progesterone induced breast precancerous lesions rats by PI3K/AKT/mTOR signaling pathway. ResearchGate 2021.

[7] Li DH, Su YF, Fan HF, et al. Effect of Xihuang Pill on microcirculation in DMBA combined estrogen and progesterone induced breast precancerous lesions rats. IOP Conf. Ser.: Earth Environ. Sci 2020;474(5):52053–52055.

[8] Li DH, Su YF, Fan HF, et al. Xihuang pill reversing precancerous lesions of breast cancer in rats and regulating the expression of NF-kappa B protein. Chinese Journal of Gerontology 2021;41(1):131-134.

[9] Mao D, Feng L, Huang SQ, Zhang SF, Peng WJ, and Zhang SF. Meta-Analysis of Xihuang Pill Efficacy When

Combined with Chemotherapy for Treatment of Breast Cancer. Evidence-based complementary and alternative medicine 2019;2019:Article ID 3502460, 14 pages.

[10] Wu YP, Zhou Y, Pu J, Li H, Zhang JG, and Zhu YP. Application Progress of Metabolomics in Tumor Drug Target Screening. Biotechnology Bulletin 2022:1-8.

[11] Pang B, Liu S, Liu ZQ, Liu SY, and Song FR. Application of Microdialysis Combined with Liquid Chromatography- Mass Spectrometry Technique on Chinese Medicine Research. Journal of Chinese Mass Spectrometry Society 2021;42(5):553-562.

[12] Mohammed FS, Ghosh A, Pal S, et al. Hydroalcoholic Extract of Sechium edule Fruits Attenuates QT Prolongation in High Fat Diet-Induced Hyperlipidemic Mice. Evidence-Based Complementary and Alternative Medicine 2022;2022:1-7.

[13] Taifa S, Muhee A, Bhat RA, et al. Evaluation of Therapeutic Efficacy of Copper Nanoparticles in Staphylococcus aureus-Induced Rat Mastitis Model. Journal of Nanomaterials 2022;2022:1-12.

[14] Khan A, Ahmed QU, Narayanamurthy V, et al. Anticancer activity of grassy Hystrix brachyura bezoar and its mechanisms of action: An in vitro and in vivo based study. Biomedicine & pharmacotherapy= Biomedecine & pharmacotherapie 2019:114:108841.

[15] Xu L, and Cao Y. Native musk and synthetic musk ketone strongly induced the growth repression and the apoptosis of cancer cells. BMC complementary and alternative medicine 2016:16(1):511.

[16] Wang C, and Lou YN. Clinical and experimental research progress of Xihuang Pill in the treatment of breast cancer. Journal of China-Japan Friendship Hospital 2020;34(3):170-172.

[17] Wu EB, Yang HB, Lu YF, et al. Effects of deoxycholic acid on apoptosis of human gastric cancer BGC-823 cells. Guangdong Medical Journal 2016;37(12):1795-1798.

[18] Guo SX, Liu YH, Chang J, et al. Expressions of Angiogenic Factors in Breast Cancer with Blood Stasis By Musk Ketone Intervention. Journal of Hebei Traditional Chinese Medicine and Pharmacology 2011;26(2):40-41.

[19] Chen YL, Zhou CL, Ge ZD,et al. Composition and potential anticancer activities of essential oils obtained from myrrh and frankincense. Oncology letters 2013;6(4):1140-1146.

[20] Cai HD, Su SL, Zhou W, et al. Research progress in boswellic acids from medicinal plants in Boswellia Roxb. ex Colebr. and their pharmacological action as well as mechanisms. Chinese Traditional and Herbal Drugs 2016;47(12):2175-2181.

[21] Gathungu RM, Kautz R, Kristal BS, et al. The integration of LC-MS and NMR for the analysis of low molecular weight trace analytes in complex matrices. Mass Spectrom Rev 2020;39(1-2):35-54.

[22] Li Q, and Kang C. A Practical Perspective on the Roles of Solution NMR Spectroscopy in Drug Discovery. Molecules (Basel, Switzerland) 2020;25(13):2974.

[23] Li Y, and Kang C. Solution NMR Spectroscopy in Target-Based Drug Discovery. Molecules (Basel, Switzerland) 2017;22(9):1399.

[24] Kumar D, Gupta A, Mandhani A, and Sankhwar SN. NMR spectroscopy of filtered serum of prostate cancer: A new frontier in metabolomics. The Prostate 2016;76(12):1106-1119.

[25] Li SB, Tian YF, Jiang PYZ, et al. Recent advances in the application of metabolomics for food safety control and food quality analyses. Critical reviews in food science and nutrition 2021;61(9):1448-1469.

[26] Yan XY, and Gao JZ, Application of MALDI-TOF MS in the early diagnosis of non-small cell lung cancer. The Journal of Medical Theory and Practice 2022;35(9):1478-1481.

[27] Guo TY. Research Progress on the pharmacological action of abscisic acid. Electronic Journal of Clinical Medical Literature 2017;4(77):15239+15242.

[28] Zhao HW, Li LJ, Pan J, Han B, and Xia H. Apoptosis of Tca8113 Squamous Cell Car cinoma Cells Induced by Abscisic Acid in Animal Models. Chinese Journal of Clinical Oncology 2008;35(9):523-526.

[29] Zhang H, Lao XZ, Li HQ, and Zheng H. Research advances in pharmacological function and molecular target of abscisic acid. Biotic Resources 2017;39(5):322-327.

[30] Jung YH, Cackowski FC, Yumoto KJ, et al. Abscisic acid regulates dormancy of prostate cancer disseminated tumor cells in the bone marrow. Neoplasia 2021;23(1):009.

[31] Jang DS, Cuendet M, Pawlus AD, et al. Potential cancer chemo- preventive constituents of the leaves of Macaranga triloba. Phy- tochemistry 2004;65(3):345-350.

[32] Wojcieszyńska D, and Guzik U. Naproxen in the environment: its occurrence, toxicity to nontarget organisms and biodegradation. Appl Microbiol Biotechnol 2020;104(5):1849-1857.

[33] Hao LF, Chen Y, Huang YP, and Liu ZS. Study of release on the moleculary imprinted polymer for S-naproxen. Journal of Tianjin Medical University 2009;15(3):345-347.

[34] Patrignani P, and Patrono C. Cyclooxygenase inhibitors: From pharmacology to clinical read-outs. Biochimica et biophysica acta 2015;1851(4):422-432.

[35] Li ZJ, Chen Y, Wang QP, et al. Research Progress of Anti-Inflammatory Platinum(IV) Complexes as Antitumor Drugs. Journal of Liaocheng University(Natural Science Edition) 2020;33(5):97-103.

[36] Liu TT, and Yu SP. Research progress in the regulation of glucose and lipid metabolism by sirtuin2. Journal of Jining Medical University 2017;40(1):59-62.

[37] Bian XL, Liu R, Meng Y, et al. Lipid metabolism and cancer. The Journal of experimental medicine 2021;218(1): e20201606.

[38] Wang AM, and Chen SZ. Effect of adipose tissue microenvironment on tumor biology. Chinese Medicinal Biotechnology 2021;16(6):539-545.

[39] Dunneram Y, Greenwood DC, and Cade JE. Diet, menopause and the risk of ovarian, endometrial and breast cancer. The Proceedings of the Nutrition Society 2019;78(3):438-448.

[40] Ko SH, and Kim HS. Menopause-Associated Lipid Metabolic Disorders and Foods Beneficial for Postmenopausal Women. Nutrients 2020;12(1):202.

[41] Cha YJ, Kim ES, and Koo JS. Amino Acid Transporters and Glutamine Metabolism in Breast Cancer. International journal of molecular sciences 2018;19(3):907.

[42] Gao HM, and Yang SY. Research progress of tumor amino acid metabolism. Medical & Pharmaceutical Journal of Chinese People's Liberation Army 2021;33(8):112-116.

[43] Chi AP, Kang YJ, Zhang Y, et al. Urinary metabolomics study of Epimedium polysaccharide for the treatment of chronic fatigue rats. Journal of Shaanxi Normal University(Natural Science Edition) 2017;45(2):116-124.

[44] Lina S, Lise B, Elizabeth SB, et al. Human steroid biosynthesis, metabolism and excretion are differentially reflected by serum and urine steroid metabolomes: A comprehensive review. J Steroid Biochem Mol Biol 2019;194:105439.

[45] Zhou XN, Yang LH, Li ZM, Duan Y, Zhou T, and Hu KW. Discussion on the Clinical Application of Xingxiao Pills in the Treatment of Malignant Tumor. Journal of Guangzhou University of Traditional Chinese Medicine 2021;38(8):1745-1749.

[46] Ge AQ, Yang KL, Liu LF, Zeng LT, and Fan HQ. A Network Pharmacology Approach to Explore the Molecular Mechanism of RU XIANG-MO YAO Pair on Breast Hyperplasia. Modernization of Traditional Chinese Medicine and Materia Medica-World Science and Technology 2020;22(4):914-925.

[47] Wang Y., Qiao JJ, Zhang L, Liu SW, and Yang SC. The role of steroid hormones in breast cancer and its effect on cancer stem cells. Practical Oncology Journal 2019;33(5):466-470.

[48] Paulsen O, Klepstad P, Rosland JH, et al. Efficacy of methylprednisolone on pain, fatigue, and appetite loss in patients with advanced cancer using opioids: a randomized, placebo-controlled, double-blind trial. J Clin Oncol 2014;32(29):3221-3228.

[49] Wu ZG, Yin WX, Luo HL, Si YK, Sun MQ, and Liao LC. Metabolic abnormalities associated with ketamine-associated bladder toxicity based on metabolomics. Acta Pharmaceutica Sinica 2020;55(8):1849-1854.

[50] Zhong SJ, Li J, Li L, et al. Study on The Biological Mechanism of Diseases due to Salty Taste Based on Urine Metabonomics. Journal of Basic Chinese Medicine 2021;27(6):950-953+1003.

[51] Qi B, Wu SG, Wang J, Qi GH, and Zhang HJ. Physiological Function and Its Application in Animal Feeding of β-Alanine. Chinese Journal of Animal Nutrition 2016;28(4):1027-1034.

[52] Gaunitz F, and Hipkiss AR. Carnosine and cancer: a perspective. Amino acids 2012;43(1):135-142.

[53] Chen T, Xu SY, and Feng Y. Inducing Conditions of Recombined L-aspartate-α-decarboxylase in Fermentor. Journal of Jinling Institute of Technology 2016;32(3):80-83.

[54] Saunders B, Elliott-Sale K, Artioli G. G, et al. β-alanine supplementation to improve exercise capacity and performance: a systematic review and meta-analysis. Br J Sports Med 2017;51(8):658-669.

[55] Gemeli T, De Andrade RB, Rojas DB, et al. Chronic exposure to beta-alanine generates oxidative stress and alters en ergy metabolism in cerebral cortex and cerebellum of Wistar rats. Mol Neurobiol 2018;55(6):5101-5110.

[56] Xu Y. The Mechanism research of Xihuang Pills Inhibiting Tumor Growth in Breast Tumor-bearing Mice by Regulating Amino Acid Metabolism. Dalian University 2018.

Figures

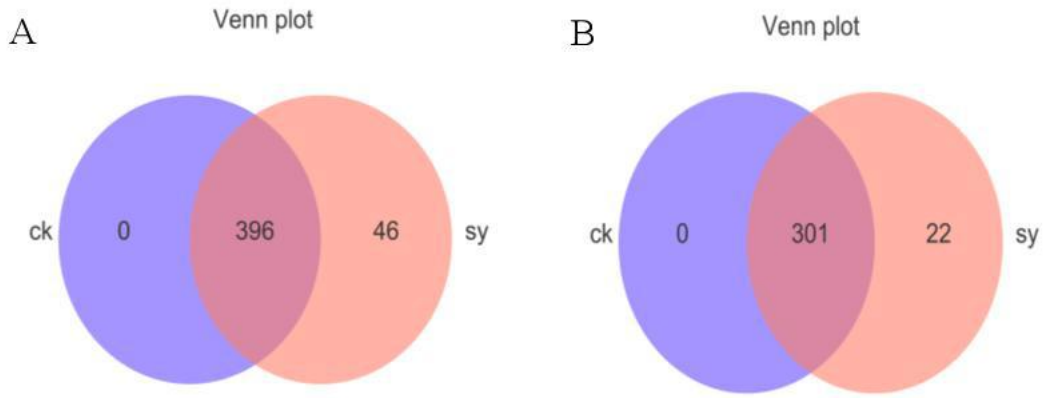

Figure 1 Veen diagram of differential metabolites.

Note: A. Positive ion mode; B. Negative ion mode.

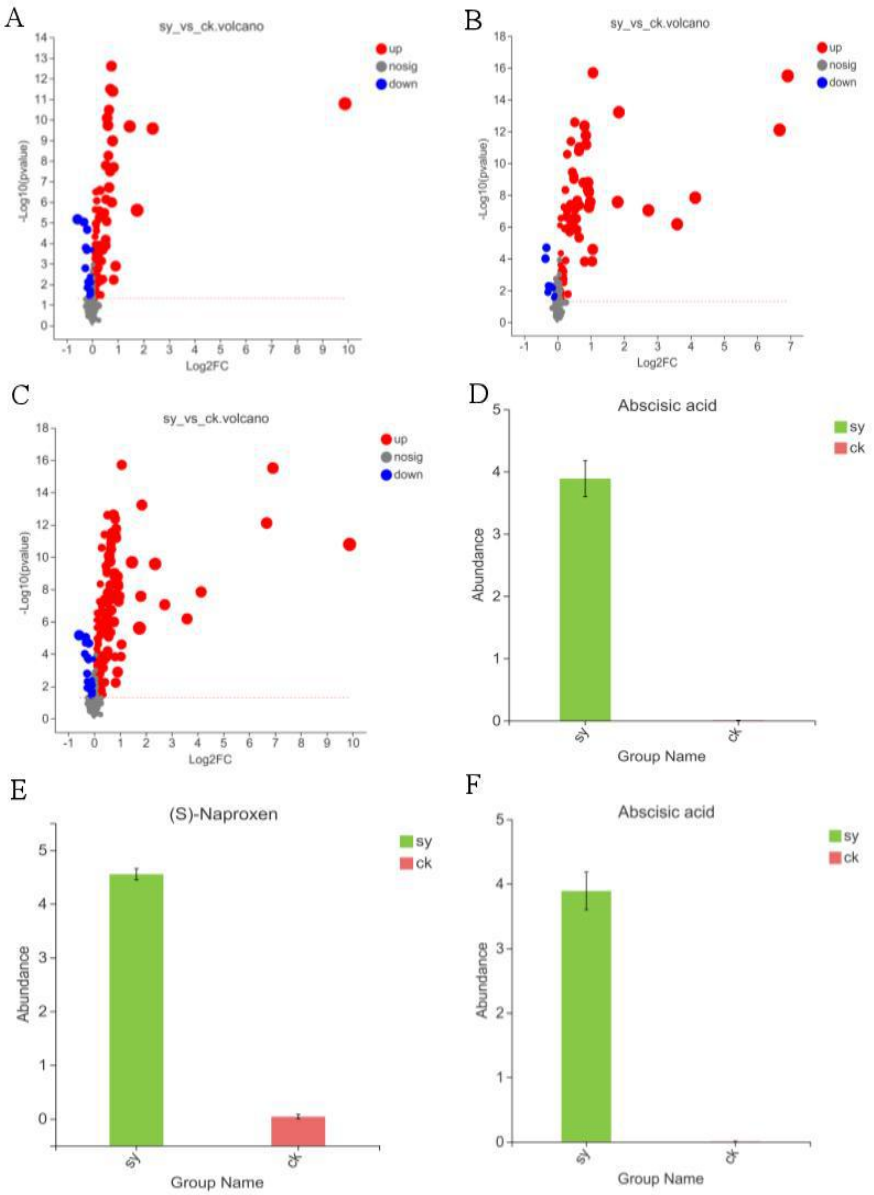

Figure 2. Two groups of difference volcano plots and abundance histograms.

Note: A. Positive ion mode; B. Negative ion mode; C. Positive-negative ion mode; D. Positive ion mode; E. Negative ion mode; F. Positive-negative ion mode.

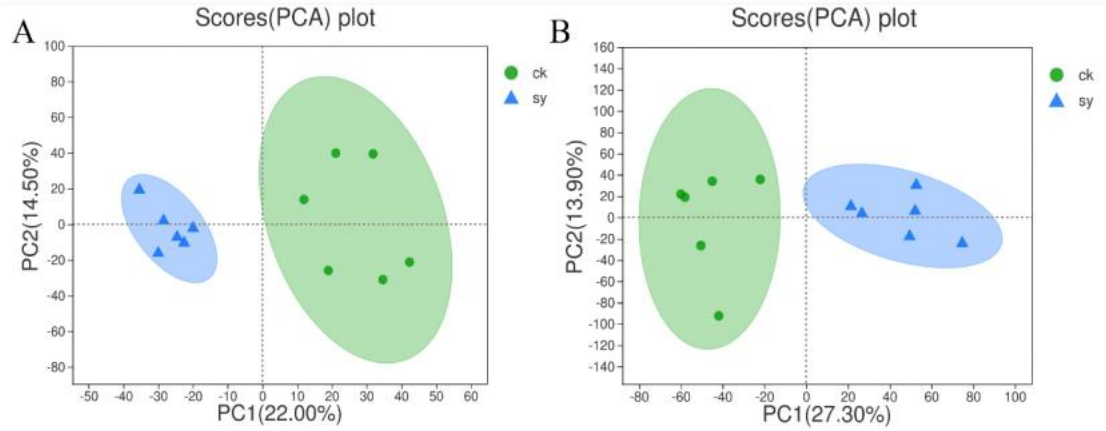

Figure 3 Two sets of PCA score chart.

Note: A. Positive ion mode; B. Negative ion mode.

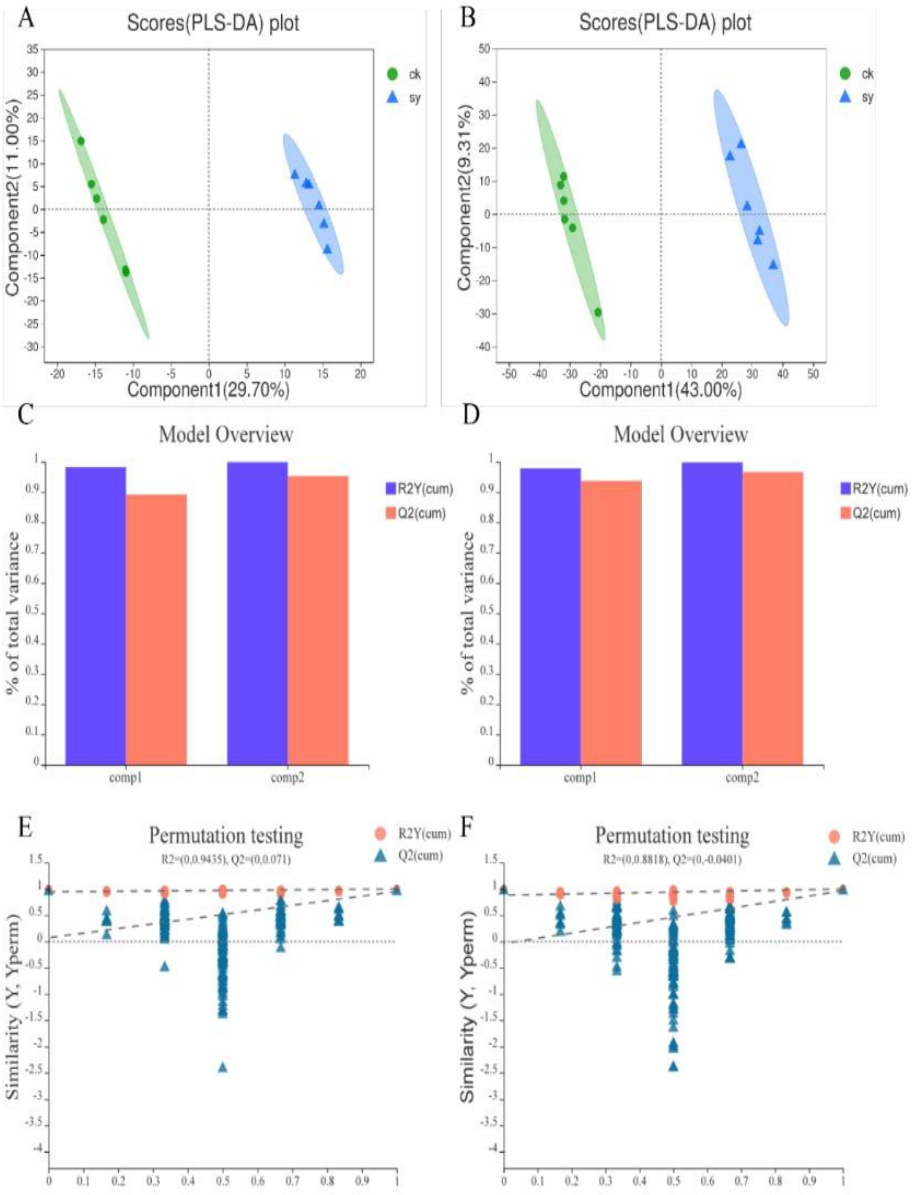

Figure 4 Two groups of PLS-DA score diagrams, model overview diagrams, and permutation test diagrams.

Note: A. Positive ion mode score diagram; B. Negative ion mode score diagram; C. Positive ion mode model overview diagram; D. Negative ion mode model overview diagram; E. Positive ion mode replacement inspection diagram; F. Negative ion mode replacement inspection diagram.

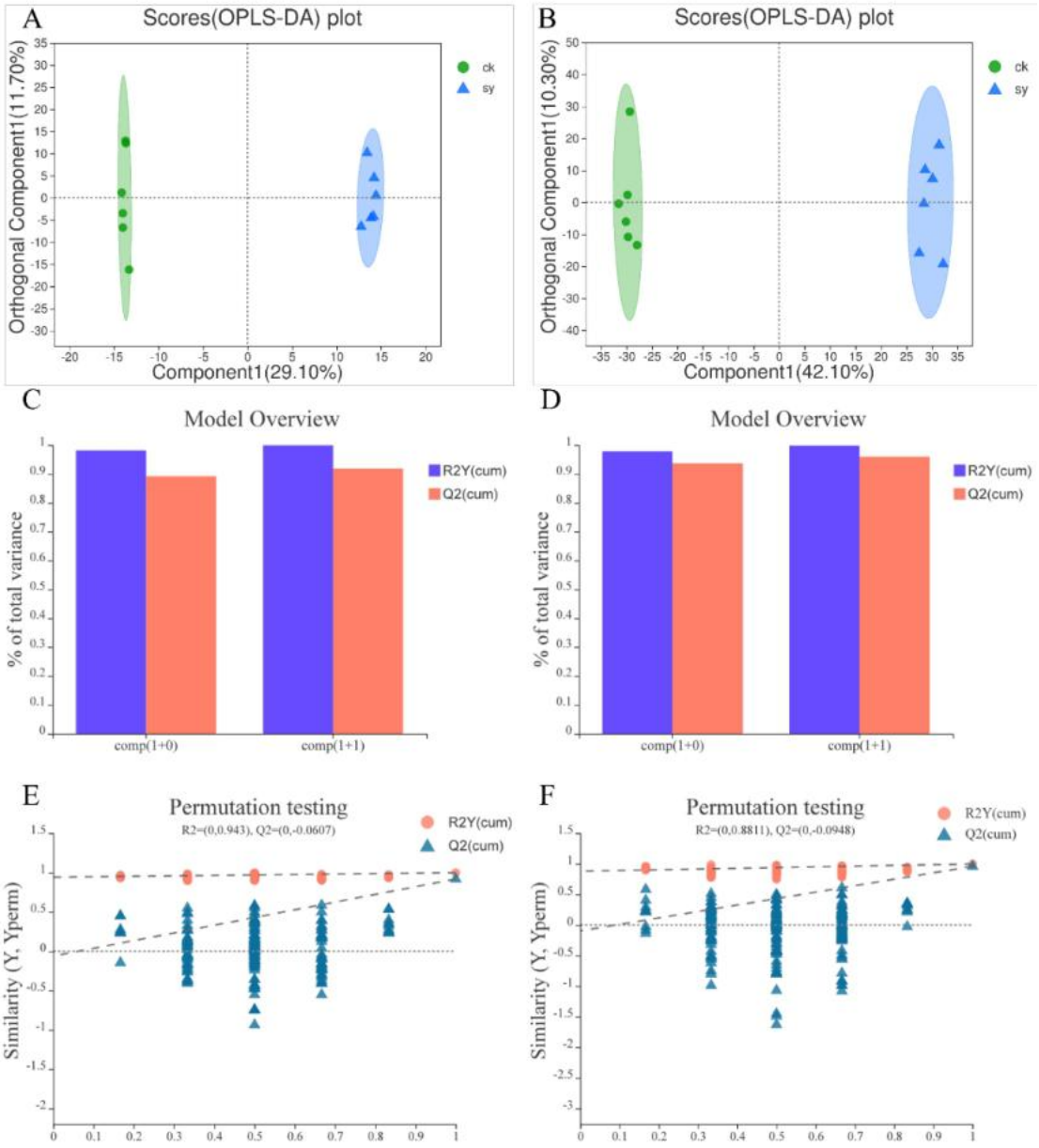

Figure 5 Two groups of OPLS-DA score diagrams, model overview diagrams and permutation test diagrams.

Note: A. Positive ion mode score diagram; B. Negative ion mode score diagram; C. Positive ion mode model overview diagram; D. Negative ion mode model overview diagram; E. Positive ion mode replacement inspection diagram; F. Negative ion mode replacement inspection diagram.

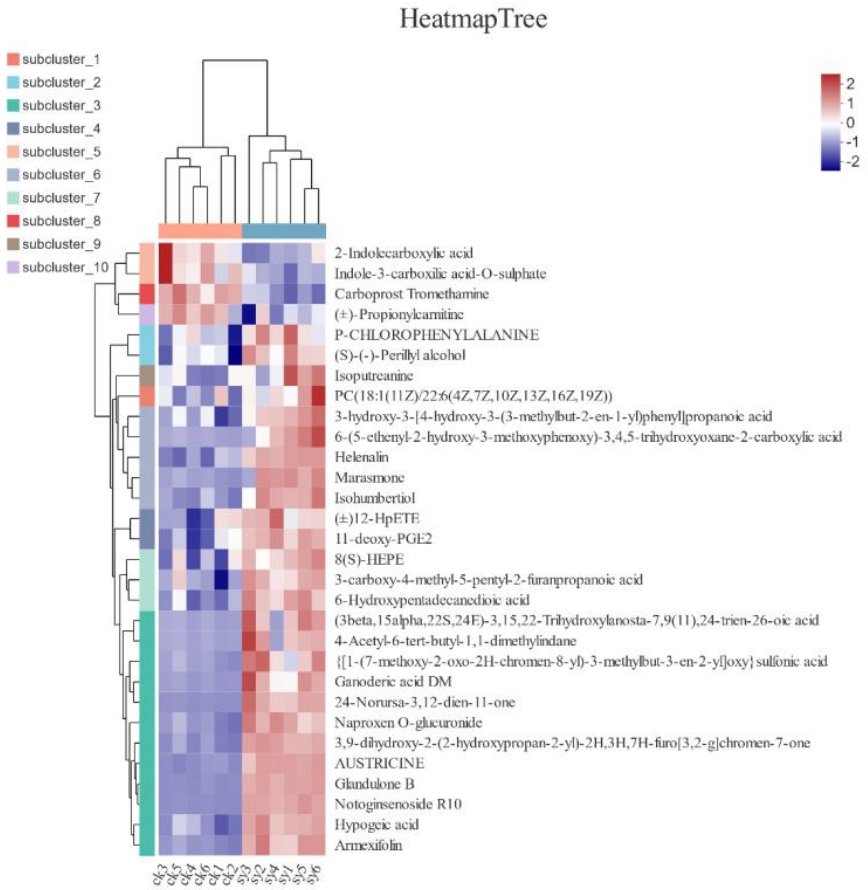

Figure 6 Metabolite cluster analysis chart.

Note: The color in the figure represents the relative expression level of the metabolite in the group of samples. The specific expression level change trend is shown in the number label under the color bar at the bottom right.

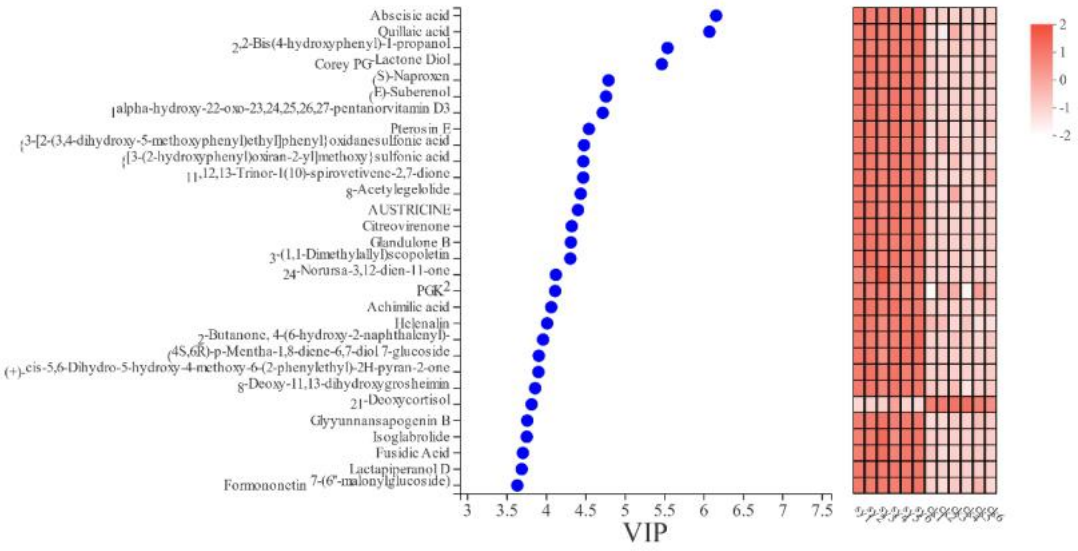

Figure 7 VIP analysis chart.

Note: On the right is the heat map of metabolite expression, each column represents a sample, and the sample name below; Each row represents a metabolite, and the color represents the relative expression level of the metabolite in the group of samples.

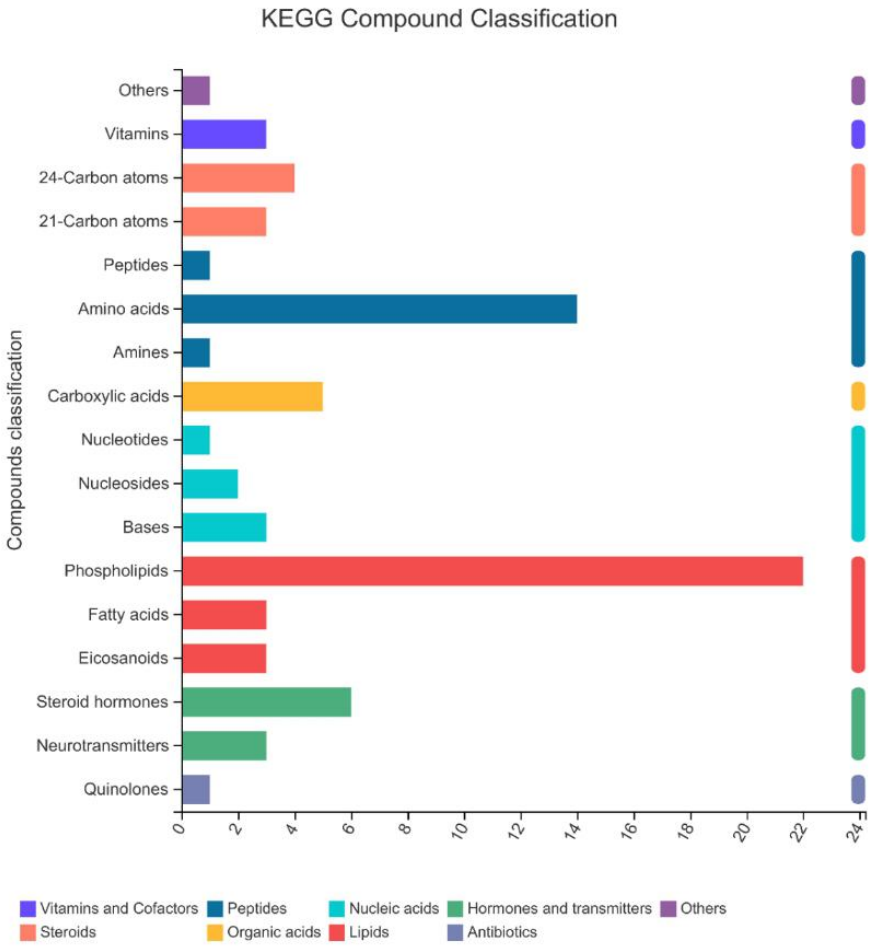

Figure 8 KEGG compound classification diagram.

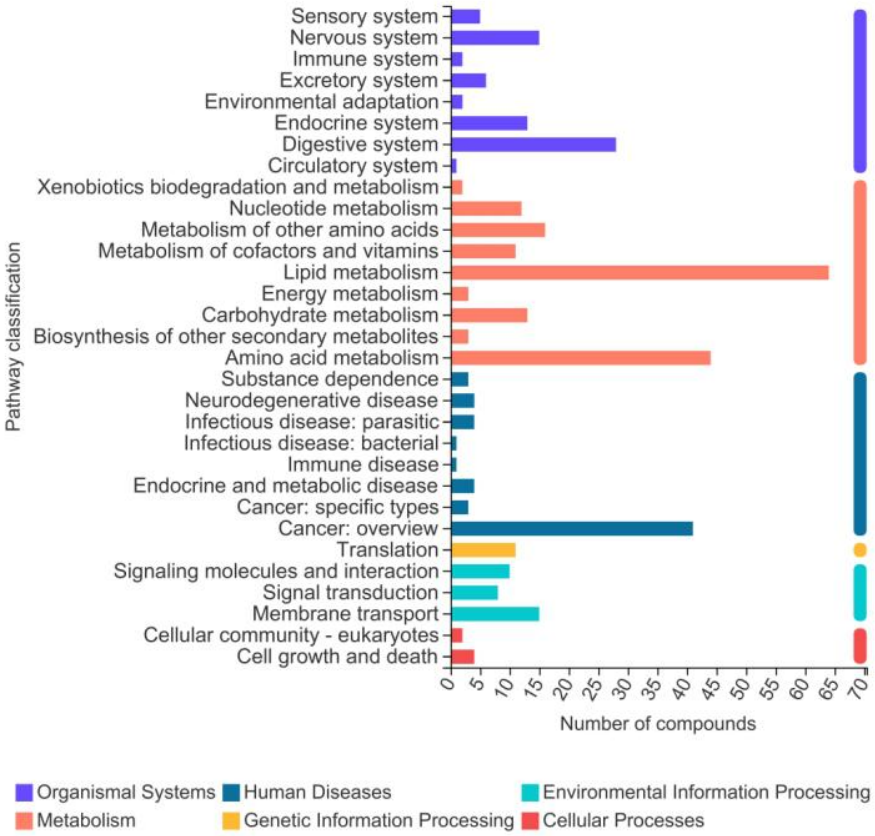

Figure 9 KEGG functional pathway diagram.

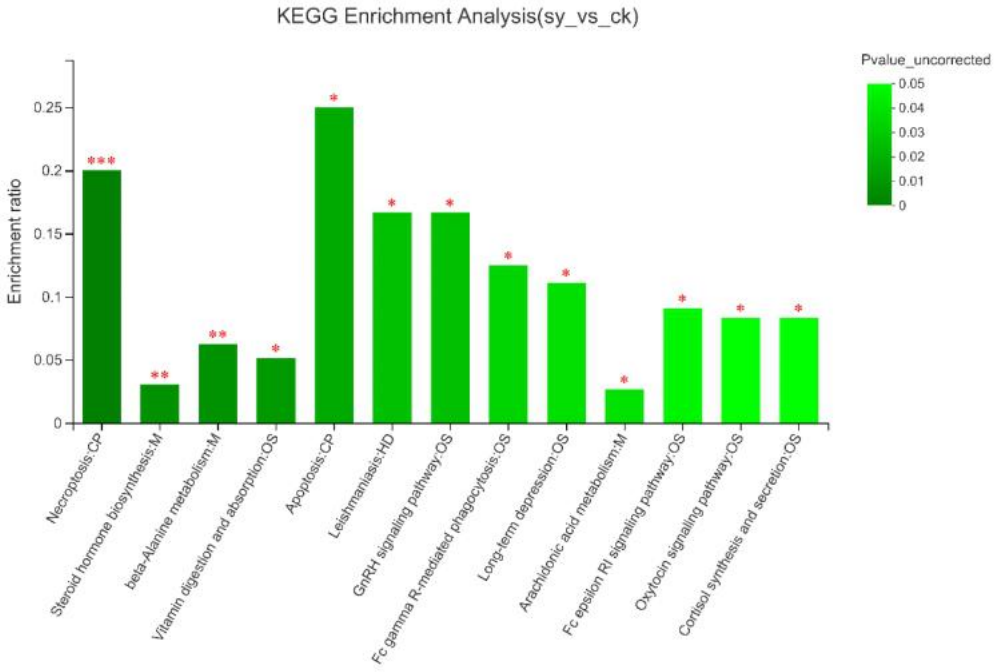

Figure 10 KEGG metabolic pathway analysis diagram.

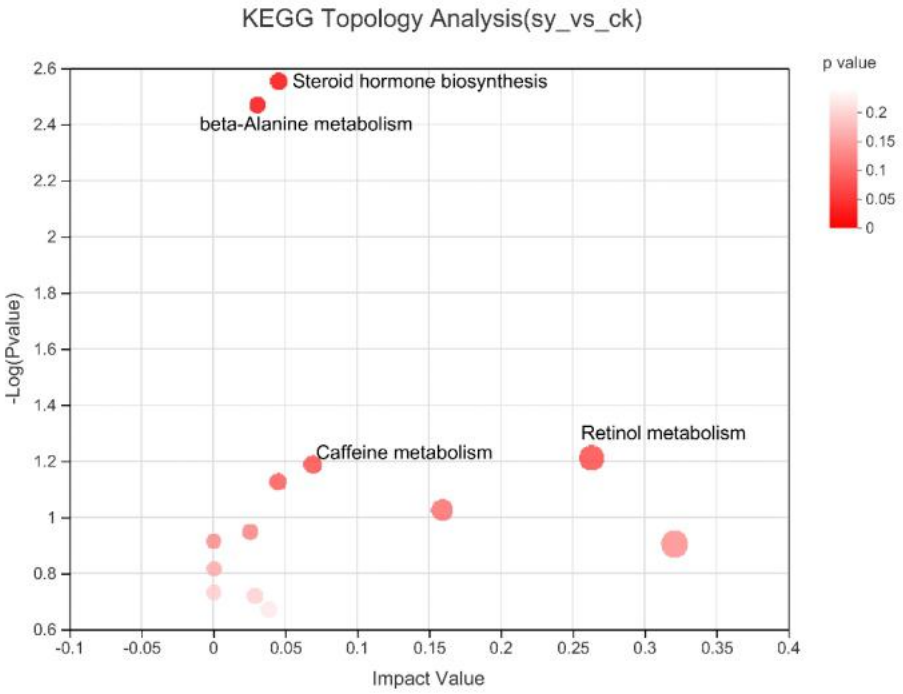

Figure 11 KEGG topology analysis path diagram.

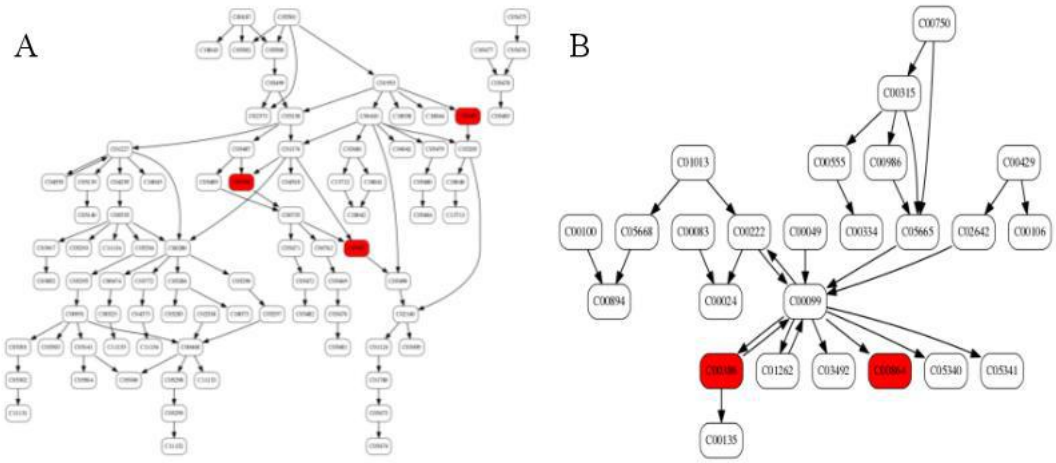

Figure 12 Network diagram of KEGG pathway in steroid hormone biosynthesis and beta-alanine metabolism.

Note: Metabolites on a white background indicate metabolites in this pathway; pathways on a red background indicate metabolites in this metabolic concentration.

Tables

Table 1. Analysis software platforms and related versions involved in this paper.

Analysis item	Software/URL	Version
Metlin database	https://metlin.scripps.edu/	no
HMDB database	http://www.hmdb.ca/	Version 5.0
Venn Diagram	Venn Diagram (R packages)	Version1.6.20
Expression data preprocessing	Majorbio's own software	no
Correlation analysis	Scipy (Python)	Version1.0.0
Differential Metabolite Analysis - Multivariate Statistics	Ropls (R packages)	Version1.6.2
PCA analysis	Ropls (R packages)	Version1.6.2
Cluster analysis	Scipy (Python)	Version1.0.0
Heatmap	Scipy (Python)	Version1.0.0
VIP analysis	Ropls (R); scipy (Python)	Version1.6.2; Version1.0.0
KEGG compound classification	https://www.kegg.jp/kegg/compound/	kegg_v 94.2
KEGG pathway enrichment	Scipy (Python)	Version1.0.0

Table 2 Serum Differential Metabolism Markers of XHP

ID	Metabolite	M/Z	Retention time	Formula	VIP_value	P_value
pos_1413	Abscisic acid	229.1222	3.9183	$C_{15}H_{20}O_4$	6.1604	1.659E-11
neg_3106	11,12,13-Trinor-1(10)-spirovetivene-2,7-dione	213.0916	5.8296	$C_{12}H_{16}O_2$	4.4739	1.438E-08
neg_2250	8-Acetylegelolide	307.1186	3.1032	$C_{16}H_{20}O_6$	4.4419	6.684E-07
pos_2847	21-Deoxycortisol	347.2211	6.0994	$C_{21}H_{30}O_4$	3.8185	0.000006894
pos_1437	2,2-Bis(4-hydroxyphenyl)-1-propanol	245.1168	4.2623	$C_{15}H_{16}O_3$	5.543	2.675E-10
neg_7754	{3-[2-(3,4-dihydroxy-5-methoxyphenyl)ethyl]phenyl}oxidanesulfonic acid	339.0543	4.3228	$C_{15}H_{16}O_7S$	4.484	8.945E-08
pos_1615	Quillaic acid	487.3413	6.5588	$C_{30}H_{46}O_5$	6.0746	0.000002508
pos_646	Corey PG-Lactone Diol	269.1745	5.3919	$C_{15}H_{24}O_4$	5.4712	2.113E-10
pos_1583	PGK2	351.2157	6.2181	$C_{20}H_{30}O_5$	4.1175	0.001304
neg_2304	{[3-(2-hydroxyphenyl)oxiran-2-yl]methoxy}sulfonic acid	245.0122	3.2813	$C_9H_{10}O_6S$	4.4749	2.69E-08
neg_7701	Citreovirenone	229.0866	4.4459	$C_{14}H_{16}O_4$	4.328	6.039E-14
pos_1381	Helenalin	263.1276	3.5650	$C_{15}H_{18}O_4$	4.0153	0.000001038
pos_643	Glandulone B	245.1170	5.6671	$C_{15}H_{16}O_3$	4.3166	2.493E-13
pos_673	AUSTRICINE	263.1274	4.5786	$C_{15}H_{18}O_4$	4.4066	1.9E-10
pos_2977	3-(1,1-Dimethylallyl)scopoletin	261.1118	5.0895	$C_{15}H_{16}O_4$	4.3101	8.277E-11
pos_1604	1alpha-hydroxy-22-oxo-23,24,25,26,27-pentanorvitamin D3	345.2421	6.4991	$C_{22}H_{32}O_3$	4.721	4.111E-12
pos_1490	Pterosin E	233.1170	4.8241	$C_{14}H_{16}O_3$	4.5457	1.063E-09
pos_2481	24-Norursa-3,12-dien-11-one	409.3462	8.6280	$C_{29}H_{44}O$	4.1264	1.963E-07
pos_2740	Isoglabrolide	469.3305	6.9737	$C_{30}H_{44}O_4$	3.7569	1.663E-08
neg_3797	Glyyunnansapogenin B	487.3424	8.1855	$C_{30}H_{48}O_5$	3.7631	4.83E-09
neg_447	Formononetin 7-(6"-malonylglucoside)	515.1190	3.3125	$C_{25}H_{24}O_{12}$	3.6367	2.653E-08
neg_3897	Fusidic Acid	537.3193	8.4688	$C_{31}H_{48}O_6$	3.7078	1.584E-09
neg_7071	Lactapiperanol D	369.1917	5.9223	$C_{18}H_{28}O_5$	3.6926	1.988E-16
neg_584	8-Deoxy-11,13-dihydroxygrosheimin	261.1131	4.5816	$C_{15}H_{20}O_5$	3.8636	5.626E-08
pos_1426	Achimilic acid	279.1228	4.0935	$C_{15}H_{18}O_5$	4.0679	3.241E-12
pos_3000	(+)-cis-5,6-Dihydro-5-hydroxy-4-methoxy-6-(2-phenylethyl)-2H-pyran-2-one	249.1117	4.9490	$C_{14}H_{16}O_4$	3.9053	3.315E-11
pos_3055	2-Butanone, 4-(6-hydroxy-2-naphthalenyl)-	215.1066	4.4806	$C_{14}H_{14}O_2$	3.9638	2.035E-08
pos_3212	(4S,6R)-p-Mentha-1,8-diene-6,7-diol 7-glucoside	295.1534	3.2376	$C_{16}H_{26}O_7$	3.9105	3.238E-08
neg_7818	(S)-Naproxen	229.0866	4.1531	$C_{14}H_{14}O_3$	4.7948	3.116E-16
neg_2906	(E)-Suberenol	259.0974	5.1608	$C_{15}H_{16}O_4$	4.7632	7.869E-13